CLIMATOLOGY

A predominantly tropical influence on late Holocene hydroclimate variation in the hyperarid central Sahara

Thijs Van der Meeren[1]*, Dirk Verschuren[1], Florence Sylvestre[2], Yacoub A. Nassour[2,3], Evi L. Naudts[1], Luis E. Aguilar Ortiz[1], Pierre Deschamps[2], Kazuyo Tachikawa[2], Edouard Bard[2], Mathieu Schuster[4], Moussa Abderamane[3]

The climate history of the Sahara desert during recent millennia is obscured by the near absence of natural climate archives, hampering insight in the relative importance of southerly (tropical) and northerly (midlatitude) weather systems at submillennial time scales. A new lake sediment record from Ounianga Serir oasis in northern Chad, spanning the Late Holocene without interruption, confirms that immediately before ca 4200 years ago, the Sahara experienced an episode of hyperaridity even more extreme than today's desert climate. The hypersaline terminal lake which formed afterwards never desiccated during the late Holocene due to continuous inflow of fossil groundwater, yet its water balance was sensitive to temporal variation in local rainfall and lake surface evaporation. Our in-lake geochemical proxies show that, during the last 3000 years, century-scale hydroclimate variation in the central Sahara primarily tracked the intensity of the tropical West African monsoon, modulated at shorter time scales by weather patterns linked to shifts in midlatitude Atlantic Ocean circulation.

INTRODUCTION

The climate history of the Sahara, the world's largest warm desert, is a subject of considerable interest as much as it is difficult to achieve adequate documentation. Much of what we know of past climate dynamics in the Sahara during the Holocene (starting 11,700 years ago; 11.7 ka to present) is deduced from natural climate archives situated along its fringes (*1*–*4*), as archives with adequate continuity and age control are extremely rare in the continental interior (*3*, *5*). The last 3000 years, in particular, remain largely blank, because progressive aridification of North Africa throughout the Middle and Late Holocene (*6*) eventually led to complete desiccation of the lakes that would have accumulated climate proxy information in their sediments (*7*, *8*). Consequently, at present, virtually no data exist to assess the varying influence of southerly (tropical) and northerly (midlatitude) weather systems on Saharan climate in the last few millennia and, in turn, the relative importance of different climate forcing mechanisms operating at decadal to century time scales (*9*).

The only lakes in the Sahara known to accumulate a high-quality sedimentary record today are the Ounianga lakes in northeastern Chad (18.98°N and 20.67°E; Fig. 1) (*10*, *11*). Two desert oases named Ounianga Kebir and Ounianga Serir are classified together as a Natural World Heritage Site by the United Nations Educational, Scientific and Cultural Organization (UNESCO) because of the unique natural occurrence of 18 permanent aquatic habitats, ranging from fresh to hypersaline, despite the hyperarid climate (<25 mm mean annual rainfall) prevailing in this region (*12*). Sediment records of the Ounianga lakes are hence logical targets of study to elucidate the Late Holocene climate history of the central Sahara. Previously, detailed paleoclimate information was mainly provided by Lake Yoa at Ounianga Kebir (*10*, *13*, *14*). Lake Yoa being the deepest (26 m) of all Ounianga lakes, its sediment record is the only paleoenvironmental archive in the entire Sahara suspected to be continuous throughout the Holocene (*15*). However, the large volume of Lake Yoa and its hypersaline status during the past four millennia (*16*) preclude the hydrological sensitivity required to record the possibly modest hydroclimate variation occurring at decadal to century time scales. Consequently, this latest phase of climate and environmental history in the central Sahara has remained largely undocumented to date. Here, we fill this knowledge gap with detailed climate proxy data extracted from the sediment record of Lake Teli, the largest permanent lake at Ounianga Serir.

Today, rainfall in the Ounianga region is erratic (annual rainfall averaged ca 10 mm in the period 1970–2000) and limited to the months of July and August. This precipitation represents the extreme northern limit of the summer rainfall regime that sustains sparse Sahelian vegetation ca 300 km to the south (Fig. 1A), where annual rainfall is at least 100 mm. Most precipitation (>90%) currently reaching the North African Sahel region is generated by mesoscale convective systems that propagate westward over the continent and are linked to the position and relative strength of jets associated with the West African monsoon (WAM) (*17*). Springtime rainfall of northerly (midlatitude) origin is substantial only at high elevations on the Tibesti massif, 400 km to the northwest of Ounianga (*18*). The region's temperature regime is subtropical with monthly mean temperatures ranging from 19°C in January to 32°C in July and with a large daily temperature range of 15°C (*19*). Another important climatic feature is the Bodelé Jet, which represents the channeling of northeasterly surface winds through the low-elevation corridor between the Tibesti and Ennedi massifs in northern Chad (*20*). The Bodelé Jet attains maximum strength (8 m/s) in January, whereas it is absent or weak during July to August when surface wind convergence over North Africa is displaced farthest north (Fig. 1A). With virtually no rainfall or river inflow to compensate for massive lake surface evaporation year round, the Ounianga lakes would quickly dry out if they were not maintained by continuous spring discharge from the Nubian Sandstone Aquifer. This aquifer was last recharged in the Early Holocene (see the Supplementary Materials) (*21*) under

[1]Limnology Unit, Department of Biology, Ghent University, B-9000 Ghent, Belgium. [2]Aix-Marseille Université, CNRS, IRD, Collège de France, INRAE, CEREGE, Technopôle Méditerranéen de l'Arbois, Aix-en-Provence, France. [3]Université de N'Djaména, Faculté des Sciences Exactes et Appliquées, Département de Géologie, N'Djamena, Tchad. [4]Université de Strasbourg, CNRS, Institut Terre et Environnement de Strasbourg, UMR 7063, 5 Rue René Descartes, Strasbourg F-67084, France.
*Corresponding author. Email: thijs.vandermeeren@ugent.be

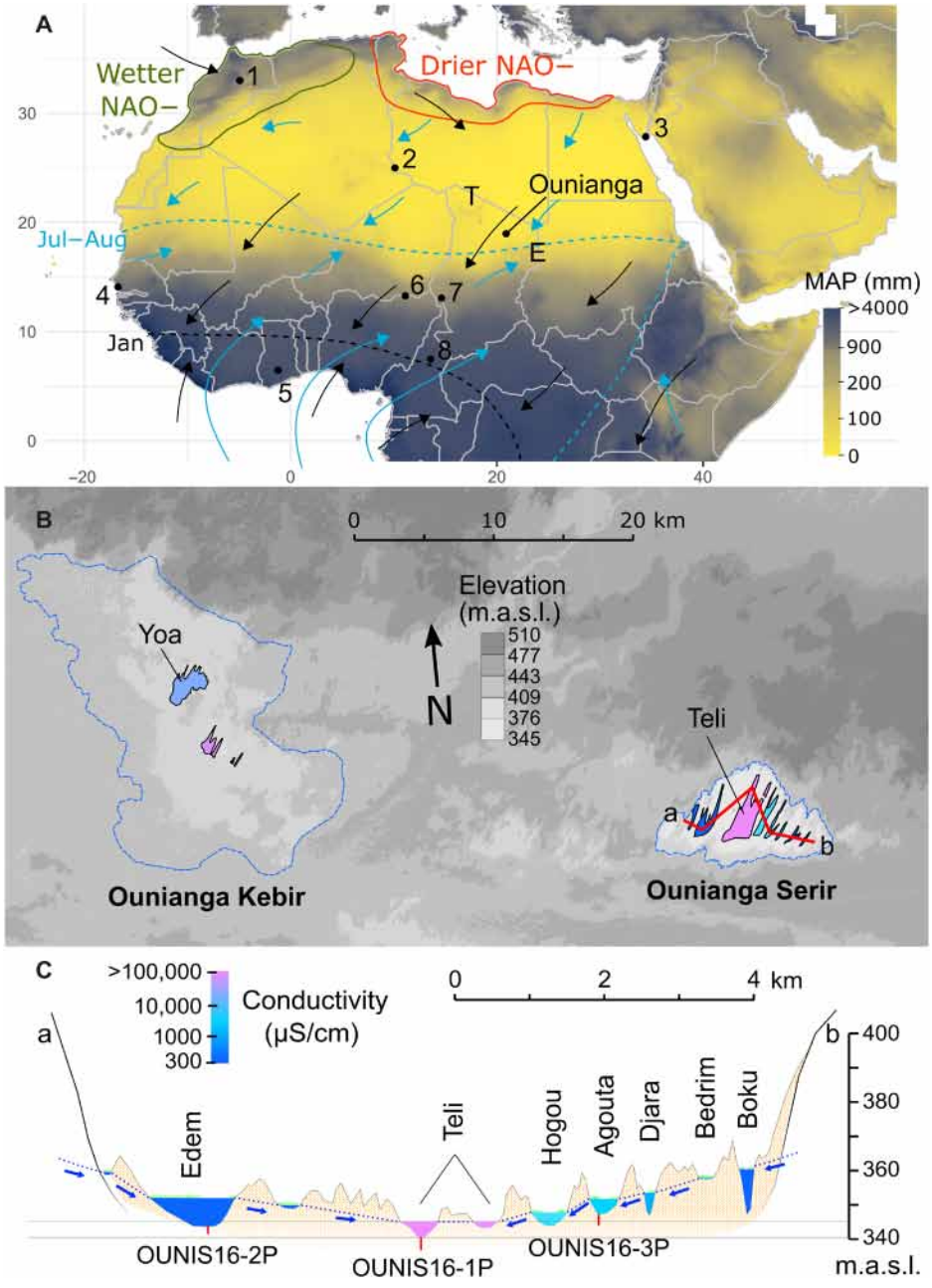

Fig. 1. Geographical and climatological setting of the Ounianga lakes. (**A**) Map of northern Africa showing the present-day distribution of mean annual precipitation (MAP; millimeters per year, nonlinear color gradient), major weather systems, and location of Ounianga in relation to the Tibesti (T) and Ennedi (E) mountains and other sites mentioned in the main text. The dashed lines indicate the position of maximum wind convergence in northern hemisphere summer (July to August) and winter (January). Blue and black arrows show the general direction and relative strength of associated winds. Green and orange contours along the southern Mediterranean coast delineate regions with respectively increased and reduced winter rainfall under a negative mode of the NAO (*45*). 1, Lake Sidi Ali (*43*); 2, Tassili N'Ajjer plateau (*40*); 3, Red Sea corals (*62*); 4, Saloum Delta shell middens (*63*); 5, Lake Bosumtwi (*6*); 6, Manga grasslands (*5*); 7, Lake Chad (*2*); 8, Lake Tizong (*42*). (**B**) Topography surrounding the deflation basins of Ounianga Kebir and Ounianga Serir at the base of the Erdi escarpment, with the estimated Early Holocene extent of both paleolakes (purple stippled lines) (*15*, *23*) and the extant lakes color coded according to their salinity (expressed as conductivity, in microsiemens per centimeter). The red line traces the transect across the Ounianga Serir basin shown in (C). (**C**) Schematic cross section of Ounianga Serir basin passing through the three OUNIS16 coring sites, with elevational position of its seven extant lakes separated by dunes (see fig. S1 for a true-color satellite image). Figure based on a regional hydrogeological map (*76*) and own terrain data. m.a.s.l., meters above sea level.

the much wetter climate conditions that prevailed during the African Humid Period (AHP; 15 to 5 ka) (*1*, *22*). At that time, most of the present-day Sahara was a grass savanna (*13*) dotted with numerous lakes and swamps interconnected by an extensive network of permanent and seasonal rivers (*7*, *8*); the two Ounianga depressions were filled by large freshwater lakes (Fig. 1B) (*10*, *23*, *24*).

Today, the largest lake of Ounianga Serir is Lake Teli (Fig. 1B), which is shallow (5 m), hypersaline (105 mS/cm specific conductance

in 2016), and lacks either surface or subsurface outflows (*15*). Analysis of short sediment records from three smaller lakes at Ounianga Serir (Edem, Agouta, and Hogou; Fig. 1C), covering the last ca 200 to 600 years, indicated fairly stable hydrological conditions at the century time scale (*11*) and thus the potential of depositional continuity over multiple millennia. Yet, analysis of Early Holocene, subrecent, and modern-day assemblages of aquatic molluscs suggested temporal discontinuity of freshwater habitat between the Early Holocene and the last few centuries (*11*, *24*), implying that Ounianga Serir oasis must have desiccated (almost) completely at least once during the Middle to Late Holocene. If substantiated, then it would imply the occurrence of a sustained past period of hyperaridity even more extreme than today's climate regime of the central Sahara desert.

Here, we reconstruct the Late Holocene paleohydrological evolution of the Ounianga Serir basin based on the radiocarbon (^{14}C) dated lake sediment record from Lake Teli. This longest and most detailed paleohydrological record is supplemented with selected sediment data from lakes Edem and Agouta. These lakes are similarly shallow (7.5 and 4.2 m); however, in contrast to Teli, they are respectively fresh and slightly brackish (0.7 and 1.8 mS/cm), because overland flow and/or seepage through the sand dunes toward Teli (Fig. 1C and fig. S1) removes dissolved salts and hence prevents strong evaporative concentration. Our hydroclimate reconstruction is mainly based on variation in the bulk composition and x-ray fluorescence (XRF) elemental ratios of the Teli record, along with the temporal distribution of diagnostic fossil remains from two groups of aquatic invertebrates (see Methods).

RESULTS

4200-year paleohydrological record from the central Sahara

Recovery of the sediment record from Lake Teli by manual push-rod coring was halted abruptly by impenetrable deposits at a sub-bottom depth of 3.8 meters. Stiff and low organic silty clays at the base of the recovered sequence (unit 0 in Fig. 2) represent a desiccation surface radiocarbon ^{14}C dated to 4.2 ± 0.2 ka [all dates mentioned are calibrated years before the present (B.P.) unless stated otherwise; fig. S3]. These clays are characterized by low water and organic matter (OM) content, elevated magnetic susceptibility (MS) values, low Ca/Ti values, and

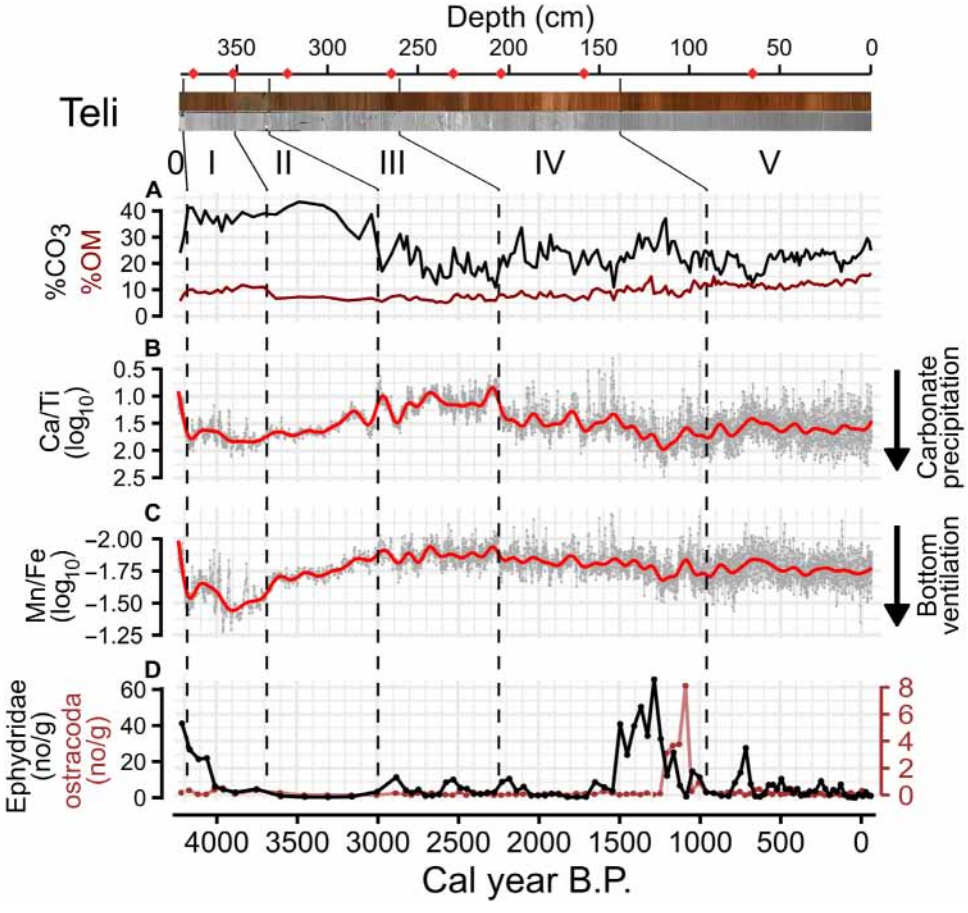

Fig. 2. 4200-year paleohydrological record of Lake Teli. Variation in geochemical and biological proxies through time with indication of the six major stratigraphic units plotted alongside digital and computed tomography (CT) images of the 3.85-m sediment sequence: (**A**) carbonate (%CO_3) and OM (%OM) content; (**B**) log-transformed (base 10) elemental ratio of Ca/Ti; (**C**) log-transformed (base 10) elemental ratio of Mn/Fe; and (**D**) density of Ephydridae remains (larval claws) and Ostracoda (valves), both expressed as abundance per gram of dry sediment. Note the reversed axes of the Ca/Ti and Mn/Fe time series, which both have a GAM smoothing function (red line) to highlight decade-scale variability. Sediment chronology is based on an age model constrained by the sediment surface (2016 CE) and eight radiocarbon (^{14}C) dates on charred grass particles, extracted from discrete depth intervals (red diamonds along the depth axis; see Methods, fig. S3, and table S1).

high XRF counts of elements reflecting detrital input (Fe, Ti, Zr, and Si) (Fig. 2 and fig. S4), all indicative of the drying and oxidation that occurs when sediments are exposed on a desiccated lake floor (*25*). Because the studied sediment record was recovered from near the deepest point of the lowest-elevation lake at Ounianga Serir (Fig. 1C), this desiccation surface implies (near) absence of aquatic habitat throughout the basin at that time (see the Supplementary Materials). Unit I comprises the first ~500 years (ca 4.2 to 3.7 ka) of lacustrine deposition following this dry stand and consists of coarsely laminated reddish brown and carbonate-rich (on average, 37.7% CO_3; range: 32.2 to 41.2%; Fig. 2) mud with high Ca/Ti and Mn/Fe values, reflecting frequent calcite precipitation in an oxygenated water column. High densities of Ephydridae (brine fly) larval remains at the base of this unit point to proximity of oxygenated hypersaline water (*26*, *27*) near the coring site, indicating that Teli was hypersaline already at the onset of this post–4.2 ka filling phase, probably due to dissolution of salt crusts that likely covered the basin floor during the dry stand. The transition to unit II is marked by decreasing values of Ca/Ti and especially Mn/Fe (Fig. 2) as well as the absence of Ephydridae remains, suggesting higher lake level and/or stronger water column stratification and consequently an increasingly anoxic lake bottom. Nevertheless, unit II (3.7 to 3.0 ka) is a rather homogeneous brown and carbonate-rich (on average, 38.8% CO_3; range: 29.2 to 43.4%) mud with low and stable OM content (6 to 7%).

Unit III (3.0 to 2.2 ka) consists of coarsely laminated, brown, and sandy carbonate mud with clayey sections. Ca/Ti and Mn/Fe stabilize at relatively low values, and the carbonate content is variable but comparatively low (on average, 19.1% CO_3; range: 10.9 to 31.2%). At the same time, Ephydridae reappear in low numbers, suggesting the occurrence of suitable habitat not too distant from the coring site. Together, these proxies indicate a lake depth not unlike that of today but stronger water column stratification. Peaks in carbonate content and Ca/Ti are dated to ca 2.9 and 2.6 to 2.4 ka (Fig. 2). Unit IV (2.2 to 0.96 ka) similarly consists of coarsely laminated and sandy carbonate mud alternating with clayey sections but is more reddish than unit III because of its higher sand and carbonate contents (on average, 23.8% CO_3; range: 11.0 to 37.1%). Maxima in carbonate and Ca/Ti are dated to ca 2.2 to 2.1, 1.7, and 1.2 ka. The progressive increases in Ca/Ti and Mn/Fe from 1.5 to 1.2 ka are accompanied by very high abundances of Ephydridae, indicating a strongly reduced lake depth and weakly stratified water column between 1.5 and 1.2 ka. At the top of unit IV, declining values of Ca/Ti and Mn/Fe and low Ephydridae numbers co-occur with a high abundance of ostracod valves (calcitic skeletal remains of mostly bottom-dwelling aquatic microcrustaceans). *Limnocythere inopinata*, the dominant species involved (>95% of ostracod remains in this section), does not normally occur in extreme hypersaline environments such as Lake Teli (see also the Supplementary Materials) (*28*) and certainly not in the anoxic or hypoxic conditions prevailing on its offshore lake bottom. Therefore, the recovered valves most likely represent a population that lived in less saline, spring-fed backwater ponds during the preceding low stand and were resuspended from muds deposited in those nearshore areas during or shortly after the transgression dated to 1.2 to 1.1 ka. Unit V (0.96 ka to present) consists of sandy but finely laminated and reddish carbonate mud (on average, 21.4% CO_3; range: 12.3 to 29.5%,), with relatively high OM content throughout (on average, 12.3%) and Ca/Ti and Mn/Fe values peaking around 0.8 ka.

Landscape evolution surrounding the modern-day desert oases at Ounianga

Two paleoenvironmental proxies extracted from Lake Teli sediments do not reflect in-lake processes but trace changes in the terrestrial environment surrounding the Ounianga Serir basin. Close temporal congruence between these landscape indicators as recorded in Lake Teli (this study) and in Lake Yoa at Ounianga Kebir 50 km to the west (Fig. 1B) (*10*, *14*) imply that climate-driven changes in vegetation cover and surface hydrology resulted in highly similar late Holocene landscape evolution at both oases. In turn, this temporal congruence between the paleoenvironmental records from lakes Yoa and Teli provides strong support for the robustness of their independently established ^{14}C-based chronologies (this study; fig. S3) (*10*). In particular, the Yoa and Teli records display congruent temporal variation in potassium (K) counts ($R = 0.57$, $P < 0.001$; fig. S5), a proxy for detrital mineral input (*29*), which, in this desert setting, is at least partly aeolian and therefore likely a representative for the wider Ounianga region. Second, the transition from clayey lake muds totally lacking sand-sized mineral particles (units 0, I, and II) to increasingly higher proportions of coarse silt and sand in units III, IV, and V (fig. S6) reflects the development of sand dunes at Ounianga Serir from ca 2.7 ka onward and their gradual encroachment of its surface waters (fig. S1) toward the present. Dune development at Ounianga Kebir progressed through time in a highly similar manner (fig. S6) (*10*).

DISCUSSION

Late Holocene hydroclimate evolution of the central Sahara

The sediment record of Lake Yoa at Ounianga Kebir (*10*, *14*) revealed hydrological and vegetation responses in the central Sahara to the marked decline in climatic moisture balance over the last 6000 years (*1*, *3*), thereby reinvigorating the long-standing debate about whether Mid-Holocene drying of the Sahara was gradual or abrupt (*22*, *30*–*32*). The data now extracted from Lake Teli at Ounianga Serir provide detailed information, heretofore lacking, on Saharan climate evolution within the last four millennia, i.e., most of the interval since the end of the AHP. Our data indicate that, immediately before ca 4200 years ago, the central basin floor of Ounianga Serir must have been completely desiccated, implying that open-water aquatic habitat, if present, only remained in areas of spring discharge along the basin's periphery. This result supports the hypothesis, based on mollusk assemblages, that the basin's aquatic habitats have experienced temporal discontinuity (*11*, *24*), thereby countering the idea that the modern-day Serir oasis contains relict aquatic habitats dating back to the AHP (*15*). The timing of Lake Teli's most recent complete desiccation notably aligns with the well-known 4.2-ka event, a possibly near-global climate anomaly (*33*) that is widely expressed as a dry spell at other Sahara oases, at lakes across the Sahel, and at other tropical areas of North Africa (*2*, *5*, *34*–*38*). The transgression of Lake Teli immediately following this dry spell corresponds with a temporary return to wetter conditions across the Sahara and Sahel (*5*, *8*, *36*), which has been broadly dated to the period 4.2 to 3.2 ka. The Late Holocene high stand of Lake Chad dated to ca 3 ka (*2*, *38*) is also an expression of this modestly wetter episode. Combined with the available evidence of Saharan climate evolution through the Holocene (*8*, *36*), our data indicate that the 4.2-ka event may represent the most extreme drought that the Sahara desert has experienced in the last 11,000 years.

In broad agreement with the continent-wide synthesis, which suggests that modern-day hyperarid conditions in the Sahara were established ca 3.2 ka (*8*, *36*), evidence for sand mobilization at Yoa and Teli from 2.7 ka onward points to the establishment of present-day atmospheric circulation patterns in the Ounianga region around that time (*10*). Before ca 3000 years ago, fluviatile sediment input to the Ounianga basins must also have been substantial (*13*, *14*). Combined with the probable erosion and redeposition of subaerially exposed early Holocene lacustrine deposits (see the Supplementary Materials), this multiplicity of sediment sources complicates climatic interpretation of geochemical proxies deposited in Lake Teli during that time. We therefore limit our hydroclimatic inferences to the portion of the Teli sequence deposited within the last three millennia. Although, during this time, the dominant regime of northeasterly harmattan winds (blowing most strongly in winter months) (*39*) implies a substantial contribution of aeolian sources to lacustrine sedimentation (*14*), gradual encroachment of Ounianga Serir by permeable sand dunes (fig. S1) is not likely to have overridden its basin-wide response to climate-driven water balance variation.

The strong positive correlation between Ca/Ti (reflecting the intensity of carbonate deposition) and Mn/Fe (reflecting water column oxygenation) throughout units III to V, both in raw ($R = 0.67$, $P < 0.001$) and generalized additive model (GAM)–smoothed data ($R = 0.91$, $P < 0.001$), suggests that the Ca/Ti ratio in Lake Teli sediments can be used as proxy for climate-driven variation in the water balance of Ounianga Serir over the last 3000 years. The Teli Ca/Ti record and associated other proxies (%CO_3 and Mn/Fe) indicate that pronounced hydroclimatic variability also occurred within the last three millennia, with major drought episodes dated to ca 2.9 to 2.8, 2.6 to 2.5, 2.2 to 2.1, 2.0 to 1.9, 1.7, 1.3 to 1.2, and 0.8 ka (Fig. 3 and fig. S8). The 1.2-ka low stand is the most pronounced and corresponds with the (near) desiccation of Lake Agouta as inferred from the age of the basal mud just above the nonrecovered desiccation horizon (fig. S5 and the Supplementary Materials). This implies

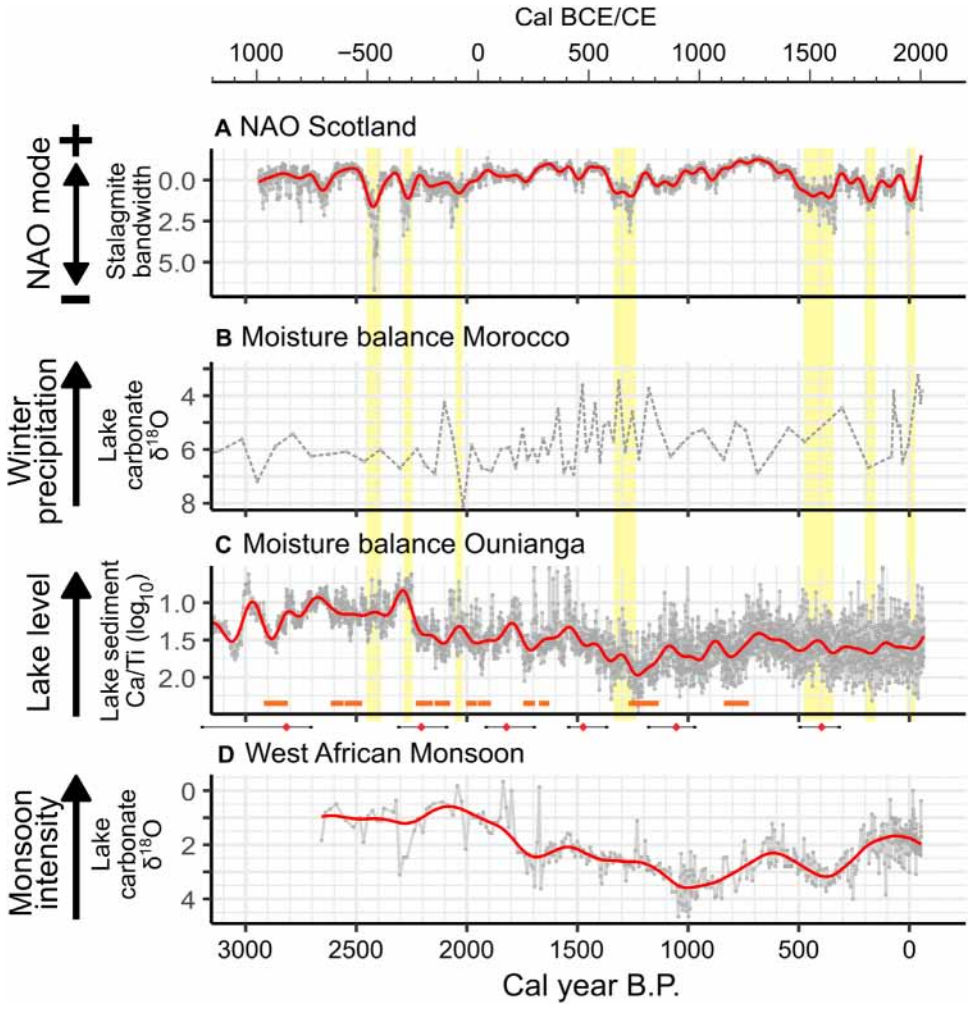

Fig. 3. Comparison of the Teli Ca/Ti time series with selected high-resolution hydroclimatic records covering the last three millennia. Climate proxy time series representing: (**A**) NAO as registered in a Scottish stalagmite (*53*); (**B**) winter precipitation in Morocco recorded in lake carbonates from Sidi Ali (*43*); (**C**) the Teli Ca/Ti record of moisture balance variation at Ounianga (this study), with indication of age model uncertainty (radiocarbon-dated depths as red diamonds with 2σ envelope) and the most pronounced century-scale episodes of sustained climatic drought (orange boxes); (**D**) intensity of the WAM recorded in lake carbonates from Lake Bosumtwi (*6*). All original data are in gray color, with a red GAM smooth added to highlight (multi)decadal trends. Yellow background shading indicates past episodes of pronounced negative NAO mode, some of which are registered as signatures of positive moisture balance in Morocco and negative in the central Sahara (see Discussion).

that, around 1200 years ago, all or most of the peripheral lakes at Ounianga Serir (but not the terminal lake Teli) must have stood dry or were transformed into reed marsh. Representing the culmination of a drying trend that appears to have started ca 1.5 ka, this timing is in close agreement with pronounced drought during the period 1.5 to 1.3 ka in the Tassili N'Ajjer region of southern Algeria (~25°N), as inferred from a discontinuous tree-ring record (site 2 in Fig. 1A) (*40*). Also around 1.5 ka, a shift to more enriched ostracod oxygen isotope values and a conspicuous rise in dust deposition at Kajemarum oasis (13°N; site 6 in Fig. 1A) indicate an abrupt change in atmospheric circulation over the Sahel (*41*). Relative drought in the period 1.5 to 1.2 ka has also been inferred for Sahel lakes in northern Nigeria and western Niger (13°N) (*5*). Still further south in northern Cameroon (7°N; site 8 in Fig. 1A), the most pronounced late Holocene low stand of Lake Tizong is dated to 1.3 ka (*42*). Thus, our high-resolution hydroclimate record confirms previous indications of drought being widespread across North Africa between ca 1.5 and 1.2 ka (450 to 750 CE), and extends documentation of its impact to over 18° latitude from wet tropical areas bordering the Gulf of Guinea to the central Sahara (Fig. 1A). Notably, this dry episode in continental North Africa is coeval with a prominent wet phase in Morocco (Fig. 3B) (*43*), an area of the western Mediterranean where predominant winter precipitation is positively related with the negative mode of the North Atlantic Oscillation (NAO; Fig. 1A).

At Ounianga, improved moisture balance following this drought allowed development of a marshy wetland at Lake Agouta from ca 1.1 ka (and probably at Edem, but our record from the latter lake starts at 0.9 ka only), with expansion of floating *Phragmites* reedbeds around the freshwater lakes (see the Supplementary Materials). These data from two peripheral Serir lakes are consistent with the Ca/Ti time series from Lake Teli (Fig. 3C), which suggests that lake-level rise from ca 1.2 ka and again in the period 0.9 to 0.7 ka culminated in a pronounced high stand 700 to 600 years ago, i.e., coeval with the onset of more open water conditions at Edem and Agouta (the units I to II transition at these two sites; fig. S5). This generally improved water balance following the pronounced 1.2-ka inferred low stand agrees well with historically documented wetter conditions in the Sahel during much of the 8th through 13th centuries CE, leading to flourishing trade and strongly organized kingdoms (*44*). Following this relatively wet phase, hydroclimate variability in the Ounianga region within the last 600 years appears to have been rather modest, with Ca/Ti variability in Teli only suggesting slightly drier conditions ca 300 years ago followed by moisture balance generally improving toward the present (Fig. 3C). This most recent wetting trend is also registered in the adjacent Lake Hogou (Fig. 1C) (*11*).

Southerly (tropical) versus northerly (midlatitude) climate dynamical influences

Evaluating hydroclimate history of the central Sahara during the last 3000 years as evidenced by sedimentary proxies of past water balance variation at Ounianga Serir and in the context of large-scale climate dynamical influences, we find a positive correlation ($R = 0.62$, $P < 0.001$; fig. S7A) between the Teli Ca/Ti ratio (detrended and logarithmically transformed) and variation in the intensity of the WAM (Fig. 3D), as inferred from carbonate oxygen isotope signatures in the sediments of Lake Bosumtwi in Ghana (6.5°N; site 5 in Fig. 1A) (*6*). At the same time, the Teli Ca/Ti record is inversely correlated ($R = -0.50$, $P = 0.001$; fig. S7B) with western Mediterranean winter precipitation (Fig. 3B), inferred from ostracod oxygen isotope signatures in the sediments of Lake Sidi Ali (also known as Lake Aguelmame Sidi Ali) in Morocco (33°N; site 1 in Fig. 1A) (*43*). In other words, at the multi-century time scale, the climatic moisture balance of the Sahara is improved (i.e., less extremely negative) when the WAM is strong and western Mediterranean winter rainfall is reduced. Conversely, the central Sahara experienced extreme aridity (e.g., ca 1300 years ago: 1.25 ka or 700 CE) when the WAM was relatively weak and western Mediterranean winter rainfall was higher than average. The broad anticorrelation between winter precipitation in Morocco and moisture balance at Ounianga (Fig. 3, B and C) suggests that the opposing moisture response manifested in western and eastern parts of the southern Mediterranean associated with the negative NAO phase (Fig. 1A) (*45*, *46*) may affect a broader region of continental North Africa. We suggest that this spatial pattern, for which there are indications that it existed on longer time scales in northwestern Africa (*47*), may extend far southward into the central Sahara, as is also indicated by climate simulations for the last millennium (*48*). However, on the basis of our results, a teleconnection whereby midlatitude westerlies interact with the subtropical manifestation of monsoon-derived moisture advection provides a more likely mechanism than a direct effect on central Saharan hydroclimate through variation in winter precipitation. Simulated variability in the WAM and Atlantic sea surface temperatures during the last millennium in fact suggest a strong link between episodes of enhanced (reduced) moisture transport into the broader Sahel region and high (low) sea surface temperatures in the North Atlantic and the Mediterranean (*9*).

The positive correlation between Teli Ca/Ti and WAM intensity suggests that conditions of somewhat tempered desert aridity during the late Holocene depended on (sub)tropical moisture penetrating far into the Sahara during summer rather than midlatitude moisture being delivered during winter, as was recently proposed to have occurred during the AHP (*49*). Also in today's climatic setting, the scarce and erratic moisture reaching Ounianga intrudes during summer months from the Sahel region to the south (*18*). Although rainfall is extremely variable between years even there and the number of active weather stations is rather low, the instrumental record depicts a rainfall dipole between the Sahel and the tropical Gulf of Guinea region (*17*). This dipole pattern is thought to arise from variation in the intensity and position of atmospheric jets associated with the intertropical convergence zone (*50*) and also features in climate simulations for the last millennium (*9*). Our results indicate that on multidecadal to century time scales this dipole may not have been the dominant mode of rainfall variation. Rather, over the last three millennia, a relatively stable atmospheric teleconnection appears to have existed between moisture balance in the central Sahara and WAM strength. On the other hand, instrumental data do reveal fairly strong teleconnections between the WAM and NAO (*51*) and between the WAM and the Atlantic Meridional Overturning Circulation (AMOC) (*52*). Despite the strong positive correlation between Saharan hydroclimate as recorded in Teli Ca/Ti and the Bosumtwi record of WAM variability ($R = 0.62$, $P < 0.001$), at least the timing of the 1.4- to 1.2-ka drought at Ounianga matches better with negative anomalies in the longest available proxy record of NAO mode (Fig. 3, A to C) (*53*). However, taken in its entirety, there is no significant linear correlation between Teli Ca/Ti and this NAO proxy record ($R = -0.03$, $P = 0.47$) nor between Teli Ca/Ti and the longest available high-resolution AMOC reconstruction ($R = -0.11$, $P = 0.44$) (*54*). However, this may partly be due to the signatures of relatively short-term NAO anomalies being overpowered by longer-term

(i.e., multidecadal and century-scale) hydroclimate trends in our lake-based climate archive, and the AMOC reconstruction (1.4 ka to present) not extending long enough to allow robust correlation with our proxy data.

Focusing on the last millennium, our Teli data support earlier suggestions based on data from lakes with sedimentologically more dynamic settings (*5*, *41*) that the period equivalent to the Medieval Climate Anomaly (ca 1000 to 700 B.P. or 950 to 1250 CE) was not particularly dry in either the Sahara or Sahel (*55*), although WAM strength was below average throughout this 300-year period (*6*). Rather, extreme drought in the central Sahara occurred ca 1.4 to 1.2 ka B.P. (550 to 750 CE). Within the last millennium, the least arid conditions in the central Sahara prevailed ca 700 to 550 B.P. (1250 to 1400 CE), i.e., coeval with the early phase of the glaciological Little Ice Age (LIA) in Europe (*56*) and with strong tropical monsoon circulation worldwide (*6*, *57*–*60*). The glaciological LIA in the European Alps relied heavily on winter precipitation (*56*), consistent with a predominantly negative NAO mode and above-average precipitation in Morocco combined with below-average precipitation in the southern central Mediterranean (*43*, *45*). During the main phase of the LIA ca 500 to 150 B.P. (1450 to 1800 CE), i.e., the episode of near-global cooling resulting from the coincidence of low solar irradiance with high frequency of explosive volcanic eruptions (*61*), aridity in the central Sahara was not particularly pronounced either, notwithstanding a weak WAM (Fig. 3) and thus presumably negligible southerly moisture supply during summer. This may indicate that LIA cooling by itself reduced lake surface evaporation and tempered the overall climatic aridity. No temperature reconstruction from within the Sahara is currently available to corroborate this hypothesis, but coral records from the Red Sea (site 3 in Fig. 1A) suggest relatively modest temperatures over the eastern Sahara and Arabian desert at least during the late 18th century CE (*62*). Alternatively, lack of a distinct wet or dry anomaly at Ounianga may be due to its mid-continental position, yielding main-phase LIA conditions intermediate between anomalously wet conditions in the western Sahel (*63*) and northwestern Africa (*43*, *46*) versus dry conditions in northeastern Africa (*62*).

The overall pattern that emerges from our high-resolution climate proxy data is that century-scale variability in the moisture balance of the central Sahara over the last 3000 years was predominantly governed by a relatively persistent positive relationship with tropical WAM intensity and modulated by shorter-term variability in weather patterns linked to shifts in midlatitude Atlantic Ocean circulation. Paleodata from Morocco and from the North Atlantic (*43*, *64*) suggest that these same dynamics may have been at play on longer time scales, even implying that the millennial-scale southward retreat of the WAM during the Middle and Late Holocene (*6*) was modulated on the century time scale by midlatitude Atlantic events (*4*, *43*, *64*). Our lake sediment record from Ounianga Serir appears to confirm such linkage between tropical and midlatitude dynamics also for the interior North African continent, distant from Atlantic Ocean forcing.

METHODS

Sediment core collection and scanning

Composite sediment cores including the intact sediment-water interface were recovered from near the depositional center of lakes Teli, Agouta, and Edem in October 2016, using gravity and push-rod operated piston corers from an anchored platform and applying state-of-the-art field curating techniques (*65*). Computed tomography (CT) images were obtained with a medical x-ray CT scanner (Siemens, SOMATOM Definition Flash) at Ghent University Hospital. After splitting, the cores were photographed and scanned using a Geotek Multi-Sensor Core Logger, followed by lithostratigraphic description. Successive core sections were cross-correlated to produce a single composite "OUNIS16" sequence for each lake, using volume-specific MS (MSκ) data collected with a Bartington MS2E point sensor (2-mm resolution). The elemental profiles were determined with an Itrax XRF scanner (Cox Analytical Systems) with a Mo tube and operated at 30 kV, 45 mA, and 15-s exposure. XRF data obtained at 0.2-mm resolution from the upper 2.3 m of finely laminated mud in the Teli record was here reduced to 0.8-mm resolution to obtain a uniform data series for the entire OUNIS16-1P sequence. The nonlaminated sediment sequences from Edem (OUNIS16-2P) and Agouta (OUNIS16-3P) were XRF-scanned at 2-mm resolution.

Selection and interpretation of XRF elemental proxies

Raw elemental counts obtained by XRF scanning were divided by 10^3 counts per second to correct for instrumental bias and a matrix effect (*66*). Following earlier work on the Yoa record (*13*) that we deemed most relevant to our present study site in a similar desert-oasis setting, we used the Ca/Ti ratio as proxy for in-lake carbonate formation, because calcium is strongly associated with the authigenic carbonate fraction while titanium is usually absent from authigenic precipitates (*67*) but commonly associated with detrital mineral input (*68*). Similarly, we interpret the Mn/Fe ratio as proxy for bottom water oxygenation (*69*), taking into account that bottom oxygenation may be impeded both by greater lake depth (i.e., higher lake surface level) and by increased salinity (*65*). Potassium (K) is often considered a proxy for clay content (*29*); however, poor correlation with this grain-size fraction in both the Yoa (*15*) and Teli (this study) records suggest that, in these desert-oasis systems, it may be a broader proxy for clastic mineral input (*29*), which includes a substantial component of aeolian input in this environment.

Sedimentological and paleoecological analysis

Contiguous 2-cm, 1-ml samples were dried and subjected to the loss-on-ignition method (*70*) to provide data on specific wet and dry weight (grams per ml), porosity (volume %) and water content (weight %), and the organic (%OM), carbonate (%CO_3), and siliciclastic fractions of dry sediment. Calculation of the carbonate fraction based on weight loss by ashing at 1000°C (*70*) assumes that it consists entirely of $CaCO_3$. Specific dry weight data were then used to convert MSκ to mass-specific MS (MSχ; expressed in SI units). Mineral grain-size analysis was performed at 21 selected depth intervals in the Teli record following analytical procedures adopted for Lake Yoa (*14*) and performed on a LS 13 320 (Beckman Coulter) after suspension in 0.03 M sodium hexametaphosphate [$(NaPO_3)_6$] to promote the dispersion of clay particles. Paleoecological analysis involved counting ostracod valves and Ephydridae larval remains sieved (250 μm) from ca 14-ml sediment samples extracted contiguously at 4-cm intervals.

Chronology

Radiocarbon (^{14}C) dating was executed on batches of cleaned macroscopic charcoal particles, sieved (150 μm), and picked from sediment samples with volumes ranging between 14 and 173 ml. To identify

core sections containing sufficient high-quality charcoal for dating, the three sediment sequences were first subjected to a full scan of charcoal abundance in 1-ml samples at contiguous 1- (Teli) or 2-cm (Agouta and Edem) increments. Eventually, adequate charcoal samples could be extracted from eight (Teli), four (Agouta) and three (Edem) depth intervals in the respective sediment sequences. The dated material (table S1) are thin flakes of charred grasses, likely including *Phragmites* (reed) of which stands line and partly cover the Ounianga Serir lakes (fig. S1). One ^{14}C date on a reed stem from the lower part of unit I in Agouta produced an erroneously young age and was not included in the age model. Independent age models (fig. S3) for the three sediment sequences were made with the Bacon package in R (*71*). Calibrated ages are reported either as calendar years in the CE or as thousands of years B.P., with 1950 CE = 0 B.P. Given their intact sediment-water interface, the core tops were anchored in 2016 CE (−66 B.P.). No attempt was made to date subrecent deposits with a fast-decaying radio isotope (^{137}Cs or ^{210}Pb) because of the exceedingly low concentrations of these elements encountered previously in the Yoa record (*10*).

Time series smoothing and correlation

GAM smoothing functions (*72*, *73*) were fitted to the time series of XRF-derived elemental data to emphasize variability at the (multi) decadal time scale. In this procedure, automatic selection objectively determines the complexity of the fitted smoothing function, thus providing a reproducible way of smoothing data (*74*). The divergence between a relatively rigid and a highly smoothed GAM model was used to objectively delineate major anomalies in Ca/Ti compared to a longer-term mean, with positive Ca/Ti anomalies spanning >100 years (with tolerance for one brief negative excursion) retained as reflecting century-scale episodes of sustained climatic drought (fig. S8). Correlations between different proxy data were calculated using the BINCOR package in R (*75*), with unsmoothed but detrended data series resampled to achieve identical time resolution. Bin-wise resampling of the last 3000 years of the Teli Ca/Ti record produced 567 correlation points (5.2-year resolution) with the corresponding NAO reconstruction (*53*), 49 correlation points (56.2-year resolution) with the 2700-year WAM reconstruction (*6*), 48 correlation points (31.2-year resolution) with the 1500-year AMOC reconstruction (*54*), and 38 correlation points (72.7-year resolution) with the reconstruction of winter precipitation in Morocco (*43*).

SUPPLEMENTARY MATERIALS

Supplementary material for this article is available at https://science.org/doi/10.1126/sciadv.abk1261

REFERENCES AND NOTES

1. P. deMenocal, J. Ortiz, T. Guilderson, J. Adkins, M. Sarnthein, L. Baker, M. Yarusinsky, Abrupt onset and termination of the African Humid Period: Rapid climate responses to gradual insolation forcing. *Quat. Sci. Rev.* **19**, 347–361 (2000).
2. S. J. Armitage, C. S. Bristow, N. A. Drake, West African monsoon dynamics inferred from abrupt fluctuations of Lake Mega-Chad. *Proc. Natl. Acad. Sci. U.S.A.* **112**, 8543–8548 (2015).
3. J. Tierney, F. Pausata, P. deMenocal, Rainfall regimes of the Green Sahara. *Sci. Adv.* **3**, e1601503 (2017).
4. L. Sha, Y. Brahim, J. Wassenburg, J. Yin, M. Peros, F. Cruz, Y. Cai, H. Li, W. Du, H. Zhang, R. Edwards, H. Cheng, How far north did the African Monsoon fringe expand during the African Humid Period? Insights from Southwest Moroccan speleothems. *Geophys. Res. Lett.* **46**, 14093–14102 (2019).
5. F. Gasse, Diatom-inferred salinity and carbonate oxygen isotopes in Holocene waterbodies of the western Sahara and Sahel (Africa). *Quat. Sci. Rev.* **21**, 737–767 (2002).
6. T. M. Shanahan, J. T. Overpeck, K. J. Anchukaitis, J. W. Beck, J. E. Cole, D. L. Dettman, J. A. Peck, C. A. Scholz, J. W. King, Atlantic forcing of persistent drought in West Africa. *Science* **324**, 377–380 (2009).
7. A. Lezine, C. Hely, C. Grenier, P. Braconnot, G. Krinner, Sahara and Sahel vulnerability to climate changes, lessons from Holocene hydrological data. *Quat. Sci. Rev.* **30**, 3001–3012 (2011).
8. J. Holmes, P. Hoelzmann, The late pleistocene-holocene African humid period as evident in lakes, in *Oxford Research Encyclopedia of Climate Science*, H. Von Storch, Ed. (Oxford Univ. Press, 2017).
9. Q. Zhang, E. Berntell, Q. Li, F. C. Ljungqvist, Understanding the variability of the rainfall dipole in West Africa using the EC-Earth last millennium simulation. *Climate Dynam.* **57**, 93–107 (2021).
10. S. Kröpelin, D. Verschuren, A. M. Lezine, H. Eggermont, C. Cocquyt, P. Francus, J. P. Cazet, M. Fagot, B. Rumes, J. M. Russell, F. Darius, D. J. Conley, M. Schuster, H. von Suchodoletz, D. R. Engstrom, Climate-driven ecosystem succession in the Sahara: The past 6000 years. *Science* **320**, 765–768 (2008).
11. M. Creutz, B. Van Bocxlaer, M. Abderamane, D. Verschuren, Recent environmental history of the desert oasis lakes at Ounianga Serir, Chad. *J. Paleolimnol.* **55**, 167–183 (2016).
12. "United Nations Educational, Scientific And Cultural Organization Convention Concerning The Protection Of The World Cultural And Natural Heritage, thirty-sixth session," *World Heritage Committee Technical Report* (WHC-12/36.COM/19) (2012).
13. A. M. Lezine, W. Zheng, P. Braconnot, G. Krinner, Late Holocene plant and climate evolution at Lake Yoa, northern Chad: Pollen data and climate simulations. *Clim. Past* **7**, 1351–1362 (2011).
14. P. Francus, H. Von Suchodoletz, M. Dietze, R. V. Donner, F. Bouchard, A. J. Roy, M. Fagot, D. Verschuren, S. Kröpelin, Varved sediments of Lake Yoa (Ounianga Kebir, Chad) reveal progressive drying of the Sahara during the last 6100 years. *Sedimentology* **60**, 911–934 (2013).
15. S. Kröpelin, The Saharan lakes of Ounianga Serir: A unique hydrological system, in *Atlas of Cultural and Environmental Change in Arid Africa*, O. Bubenzer, A. Bolten, F. Darius, Eds. (Heinrich-Barth-Institut, 2007), pp. 54–55.
16. H. Eggermont, D. Verschuren, M. Fagot, B. Rumes, B. Van Bocxlaer, S. Kröpelin, Aquatic community response in a groundwater-fed desert lake to Holocene desiccation of the Sahara. *Quat. Sci. Rev.* **27**, 2411–2425 (2008).
17. S. E. Nicholson, Climate of the Sahel and West Africa, in *Oxford Research Encyclopedia of Climate Science*, H. Von Storch, Ed. (Oxford Univ. Press, 2018).
18. O. A. Kelley, Where the least rainfall occurs in the Sahara Desert, the TRMM radar reveals a different pattern of rainfall each season. *J. Climate* **27**, 6919–6939 (2014).
19. I. Harris, P. Jones, T. Osborn, D. Lister, Updated high-resolution grids of monthly climatic observations–The CRU TS3.10 dataset. *Int. J. Climatol.* **34**, 623–642 (2014).
20. M. Todd, R. Washington, S. Raghavan, G. Lizcano, P. Knippertz, Regional model simulations of the Bodélé low-level jet of northern Chad during the Bodélé Dust Experiment (BoDEx, 2005). *J. Climate* **21**, 995–1012 (2008).
21. A. M. Hissene, Geologie und Hydrogeologie es Erdis-Beckens, NE-Tschad. *Berliner geowiss. Abh. A* **76**, 1–67 (1986).
22. J. Tierney, P.B. deMenocal, Abrupt shifts in Horn of Africa hydroclimate since the Last Glacial Maximum. *Science* **342**, 843–846 (2013).
23. C. Grenier, P. Paillou, P. Maugis, Assessment of Holocene surface hydrological connections for the Ounianga lake catchment zone (Chad). *C. R. Geosci.* **341**, 770–782 (2009).
24. B. Van Bocxlaer, D. Verschuren, G. Schettler, S. Kröpelin, Modern and early Holocene mollusc fauna of the Ounianga lakes (northern Chad): Implications for the palaeohydrology of the central Sahara. *J. Quat. Sci.* **26**, 433–447 (2011).
25. D. Verschuren, Influence of depth and mixing regime on sedimentation in a small, fluctuating tropical soda lake. *Limnol. Oceanogr.* **44**, 1103–1113 (1999).
26. F. Mees, D. Verschuren, R. Nijs, H. Dumont, Holocene evolution of the crater lake at Malha, Northwest Sudan. *J. Paleolimnol.* **5**, 227–253 (1991).
27. B. Rumes, H. Eggermont, D. Verschuren, Representation of aquatic invertebrate communities in subfossil death assemblages sampled along a salinity gradient of western Uganda crater lakes. *Hydrobiologia* **542**, 297–314 (2005).
28. C. Meisch, *Freshwater Ostracoda of Western and Central Europe* (Süßwasserfauna von Mitteleuropa, Spektrum Akademischer Verlag, 2000).
29. I. W. Croudace, R. G. Rothwell, *Micro-XRF Studies of Sediment Cores: Applications of a non-destructive tool for the environmental sciences* (Developments in Paleoenvironmental Research 17, Springer, 2015).
30. M. Claussen, C. Kubatzki, V. Brovkin, A. Ganopolski, P. Hoelzmann, H. Pachur, Simulation of an abrupt change in Saharan vegetation in the mid-Holocene. *Geophys. Res. Lett.* **26**, 2037–2040 (1999).
31. V. Brovkin, M. Claussen, Comment on "Climate-driven ecosystem succession in the Sahara: The past 6000 years". *Science* **322**, 1326b (2008).

32. S. Kröpelin, D. Verschuren, A. M. Lezine, Response to Comment on "Climate-driven ecosystem succession in the Sahara: The past 6000 years". *Science* **322**, 1326c (2008).
33. H. Weiss, Global megadrought, societal collapse and resilience at 4.2–3.9 ka BP across the Mediterranean and west Asia. *Past Global Change Mag.* **24**, 62–63 (2016).
34. J. Holmes, F. Street-Perrott, R. Perrott, S. Stokes, M. Waller, Y. Huang, G. Eglinton, M. Ivanovich, Holocene landscape evolution of the Manga Grasslands, NE Nigeria: Evidence from palaeolimnology and dune chronology. *J. Geol. Soc.* **156**, 357–368 (1999).
35. F. Gasse, Hydrological changes in the African tropics since the Last Glacial Maximum. *Quat. Sci. Rev.* **19**, 189–211 (2000).
36. P. Hoelzmann, F. Gasse, L. Dupont, U. Salzmann, M. Staubwasser, D. Leuschner, F. Sirocko, R. Battarbee, C. Stickley, Palaeoenvironmental changes in the arid and sub arid belt (Sahara-Sahel-Arabian peninsula) from 150 kyr to present. *Dev. Paleoenviron. Res.* **6**, 219–256 (2004).
37. M. Marshall, H. Lamb, D. Huws, S. Davies, R. Bates, J. Bloemendal, J. Boyle, M. Leng, M. Umer, C. Bryant, Late Pleistocene and Holocene drought events at Lake Tana, the source of the Blue Nile. *Global Planet. Change* **78**, 147–161 (2011).
38. J. Maley, Palaeoclimates of central Sahara during the early Holocene. *Nature* **269**, 573–577 (1977).
39. R. Washington, M. Todd, S. Engelstaedter, S. Mbainayel, F. Mitchell, Dust and the low-level circulation over the Bodele Depression, Chad: Observations from BoDEx 2005. *J. Geophys. Res.: Atmos.* **111**, D03201 (2006).
40. M. Cremaschi, M. Pelfini, M. Santilli, *Cupressus dupreziana*: A dendroclimatic record for the middle-late Holocene in the central Sahara. *Holocene* **16**, 293–303 (2006).
41. F. Street-Perrott, J. Holmes, M. Waller, M. Allen, N. Barber, P. Fothergill, D. Harkness, M. Ivanovich, D. Kroon, R. Perrott, Drought and dust deposition in the West African Sahel: A 5500-year record from Kajemarum Oasis, northeastern Nigeria. *Holocene* **10**, 293–302 (2000).
42. V. Nguetsop, I. Bentaleb, C. Favier, S. Bietrix, C. Martin, S. Servant-Vildary, M. Servant, A late Holocene palaeoenvironmental record from Lake Tizong, northern Cameroon using diatom and carbon stable isotope analyses. *Quat. Sci. Rev.* **72**, 49–62 (2013).
43. C. Zielhofer, A. Kohler, S. Mischke, A. Benkaddour, A. Mikdad, W. Fletcher, Western Mediterranean hydro-climatic consequences of Holocene ice-rafted debris (Bond) events. *Clim. Past* **15**, 463–475 (2019).
44. S. E. Nicholson, The methodology of historical climate reconstruction and its application to Africa. *J. African History* **20**, 31–49 (1979).
45. M. Bini, G. Zanchetta, A. Persoiu, R. Cartier, A. Catala, I. Cacho, J. Dean, F. Di Rita, R. Drysdale, M. Finne, I. Isola, B. Jalali, F. Lirer, D. Magri, A. Masi, L. Marks, A. Mercuri, O. Peyron, L. Sadori, M. Sicre, F. Welc, C. Zielhofer, E. Brisset, The 4.2 ka BP Event in the Mediterranean region: An overview. *Clim. Past* **15**, 555–577 (2019).
46. Y. Brahim, J. Wassenburg, L. Sha, F. Cruz, M. Deininger, A. Sifeddine, L. Bouchaou, C. Spotl, R. Edwards, H. Cheng, North Atlantic ice-rafting, ocean and atmospheric circulation during the Holocene: Insights from Western Mediterranean speleothems. *Geophys. Res. Lett.* **46**, 7614–7623 (2019).
47. H. Kuhlmann, H. Meggers, T. Freudenthal, G. Wefer, The transition of the monsoonal and the N Atlantic climate system off NW Africa during the Holocene. *Geophys. Res. Lett.* **31**, L22204 (2004).
48. A. Djebbar, H. Goosse, F. Klein, Robustness of the link between precipitation in North Africa and standard modes of atmospheric variability during the last millennium. *Climate* **8**, 62 (2020).
49. R. Cheddadi, M. Carré, M. Nourelbait, L. François, A. Rhoujjati, R. Manay, D. Ochoa, E. Schefuß, Early Holocene greening of the Sahara requires Mediterranean winter rainfall. *Proc. Natl. Acad. Sci. U.S.A.* **118**, e2024898118 (2021).
50. S. Nicholson, J. Grist, A conceptual model for understanding rainfall variability in the West African Sahel on interannual and interdecadal timescales. *Int. J. Climatol.* **21**, 1733–1757 (2001).
51. M. Gaetani, B. Pohl, H. Douville, B. Fontaine, West African Monsoon influence on the summer Euro-Atlantic circulation. *Geophys. Res. Lett.* **38**, L09705 (2011).
52. P. Chang, R. Zhang, W. Hazeleger, C. Wen, X. Wan, L. Ji, R. Haarsma, W. Breugem, H. Seidel, Oceanic link between abrupt changes in the North Atlantic Ocean and the African monsoon. *Nat. Geosci.* **1**, 444–448 (2008).
53. A. Baker, J. Hellstrom, B. Kelly, G. Mariethoz, V. Trouet, A composite annual-resolution stalagmite record of North Atlantic climate over the last three millennia. *Sci. Rep.* **5**, 10307 (2015).
54. M. Mann, Z. Zhang, S. Rutherford, R. Bradley, M. Hughes, D. Shindell, C. Ammann, G. Faluvegi, F. Ni, Global signatures and dynamical origins of the Little Ice Age and Medieval Climate Anomaly. *Science* **326**, 1256–1260 (2009).
55. H. Diaz, R. Trigo, M. Hughes, M. Mann, E. Xoplaki, D. Barriopedro, Spatial and temporal characteristics of climate in medieval times revisited. *Bull. Am. Meteorol. Soc.* **92**, 1487–1500 (2011).
56. J. Matthews, K. Briffa, The "Little Ice Age": Re-evaluation of an evolving concept. *Geografiska Annaler Ser. A Phys. Geogr.* **87**, 17–36 (2005).
57. G. Haug, D. Gunther, L. Peterson, D. Sigman, K. Hughen, B. Aeschlimann, Climate and the collapse of Maya civilization. *Science* **299**, 1731–1735 (2003).
58. Y. Wang, H. Cheng, R. Edwards, Y. He, X. Kong, Z. An, J. Wu, M. Kelly, C. Dykoski, X. Li, The Holocene Asian monsoon: Links to solar changes and North Atlantic climate. *Science* **308**, 854–857 (2005).
59. J. Russell, T. Johnson, Little Ice Age drought in equatorial Africa: Intertropical convergence zone migrations and El Niño–Southern Oscillation variability. *Geology* **35**, 21–24 (2007).
60. J. Tierney, J. Smerdon, K. Anchukaitis, R. Seager, Multidecadal variability in East African hydroclimate controlled by the Indian Ocean. *Nature* **493**, 389–392 (2013).
61. M. Ahmed, K. Anchukaitis, A. Asrat, H. Borgaonkar, M. Braida, B. Buckley, U. Buntgen, B. Chase, D. Christie, E. Cook, M. Curran, H. Diaz, J. Esper, Z. Fan, N. Gaire, Q. Ge, J. Gergis, J. Gonzalez-Rouco, H. Goosse, S. Grab, N. Graham, R. Graham, M. Grosjean, S. Hanhijarvi, D. Kaufman, T. Kiefer, K. Kimura, A. Korhola, P. Krusic, A. Lara, A. Lezine, F. Ljungqvist, A. Lorrey, J. Luterbacher, V. Masson-Delmotte, D. McCarroll, J. McConnell, N. McKay, M. Morales, A. Moy, R. Mulvaney, I. Mundo, T. Nakatsuka, D. Nash, R. Neukom, S. Nicholson, H. Oerter, J. Palmer, S. Phipps, M. Prieto, A. Rivera, M. Sano, M. Severi, T. Shanahan, X. Shao, F. Shi, M. Sigl, J. Smerdon, O. Solomina, E. Steig, B. Stenni, M. Thamban, V. Trouet, C. Turney, M. Umer, T. van Ommen, D. Verschuren, A. Viau, R. Villalba, B. Vinther, L. von Gunten, S. Wagner, E. Wahl, H. Wanner, J. Werner, J. White, K. Yasue, E. Zorita, Continental-scale temperature variability during the past two millennia. *Nat. Geosci.* **6**, 339–346 (2013).
62. T. Felis, M. Ionita, N. Rimbu, G. Lohmann, M. Kolling, Mild and arid climate in the Eastern Sahara-Arabian desert during the late Little Ice Age. *Geophys. Res. Lett.* **45**, 7112–7119 (2018).
63. M. Carré, M. Azzoug, P. Zaharias, A. Camara, R. Cheddadi, M. Chevalier, D. Fiorillo, A. Gaye, S. Janicot, M. Khodri, A. Lazar, C. Lazareth, J. Mignot, N. Garcia, N. Patris, O. Perrot, M. Wade, Modern drought conditions in western Sahel unprecedented in the past 1600 years. *Climate Dynam.* **52**, 1949–1964 (2019).
64. J. Repschlager, D. Garbe-Schonberg, M. Weinelt, R. Schneider, Holocene evolution of the North Atlantic subsurface transport. *Clim. Past* **13**, 333–344 (2017).
65. G. De Cort, D. Verschuren, E. Ryken, C. Wolff, R. Renaut, M. Creutz, T. Van der Meeren, G. Haug, D. Olago, F. Mees, Multi-basin depositional framework for moisture-balance reconstruction during the last 1300 years at Lake Bogoria, central Kenya Rift Valley. *Sedimentology* **65**, 1667–1696 (2018).
66. I. W. Croudace, A. Rindby, R. G. Rothwell, ITRAX: Description and evaluation of a new multifunction x-ray core scanner. *Geol. Soc. Lond. Spec. Publ.* **267**, 51–63 (2006).
67. W. M. Last, Mineralogical analysis of lake sediments. *Dev. Paleoenviron. Res.* **2**, 143–187 (2002).
68. J. F. Boyle, Inorganic geochemical methods in Palaeolimnology. *Dev. Paleoenviron. Res.* **2**, 83–141 (2002).
69. P. Wersin, P. Hohener, R. Giovanoli, W. Stumm, Early diagenetic influences on iron transformations in a fresh-water lake sediment. *Chem. Geol.* **90**, 233–252 (1991).
70. L. Bengtsson, M. Enell, Chemical analysis, in *Handbook of Holocene Palaeoecology and Palaeohydrology*, B. E. Berglund, Ed. (John Wiley and Sons, 1986), **19**.
71. M. Blaauw, J. A. Christen, Flexible paleoclimate age-depth models using an autoregressive gamma process. *Bayesian Anal.* **6**, 457–474 (2011).
72. T. Hastie, R. Tibshirani, Generalized additive models. *Stat. Sci.* **1**, 297–310 (1986).
73. S. Wood, *Generalized Additive Models: An Introduction With R* (Chapman and Hall/CRC, ed. 2, 2006), **66**, pp. 391.
74. G. Simpson, Modelling palaeoecological time series using generalised additive models. *Front. Ecol. Evol.* **6**, 149 (2018).
75. J. Polanco-Martinez, M. Medina-Elizalde, M. Goni, M. Mudelsee, BINCOR: An R package for estimating the correlation between two unevenly spaced time series. *R Journal* **11**, 170–184 (2019).
76. "Lacs d'Ounianga-Carte hydrogéologique de reconnaissance de la République du Tchad au 1:100 000, feuille hors série," Ministry of Livestock and Hydrology (2015).
77. C. Sonntag, U. Thorweihe, J. Rudolph, E. Lohnert, C. Junghans, K. Munnich, E. Klitzsch, E. Elshazly, F. Swailem, Paleoclimatic evidence in apparent ^{14}C ages of Saharian groundwaters. *Radiocarbon* **22**, 871–878 (1980).
78. C. I. Voss, S. M. Soliman, The transboundary non-renewable Nubian Aquifer System of Chad, Egypt, Libya and Sudan: Classical groundwater questions and parsimonious hydrogeologic analysis and modeling. *Hydrogeol. J.* **22**, 441–468 (2014).
79. K. Abdelmohsen, M. Sultan, M. Ahmed, H. Save, B. Elkaliouby, M. Emil, E. Yan, A. Abotalib, R. Krishnamurthy, K. Abdelmalik, Response of deep aquifers to climate variability. *Sci. Total Environ.* **677**, 530–544 (2019).
80. G. Vasseur, P. Rousseau-Gueutin, G. de Marsily, Time constant of hydraulic-head response in aquifers subjected to sudden recharge change: Application to large basins. *Hydrogeol. J.* **23**, 915–934 (2015).
81. R. Capot-Rey, *Borkou et Ounianga: étude de géographie régionale* (Université d'Alger, 1961).
82. B. Rumes, T. Van der Meeren, K. Martens, D. Verschuren, Distribution and community structure of Ostracoda (Crustacea) in shallow waterbodies of southern Kenya. *Afr. J. Aq. Sci.* **41**, 377–387 (2016).

83. F. Mezquita, J. R. Roca, J. M. Reed, G. Wansard, Quantifying species–environment relationships in non-marine Ostracoda for ecological and palaeoecological studies: examples using Iberian data. *Palaeog. Palaeoclim. Palaeoecol.* **225**, 93–117 (2005).
84. S. Mischke, U. Herzschuh, G. Massmann, C. Zhang, An ostracod-conductivity transfer function for Tibetan lakes. *J. Paleolimnol.* **38**, 509–524 (2007).
85. T. Van der Meeren, S. Mischke, N. Sunjidmaa, U. Herzschuh, E. Ito, K. Martens, D. Verschuren, Subfossil ostracode assemblages from Mongolia–Quantifying response for paleolimnological applications. *Ecol. Ind.* **14**, 138–151 (2012).

Acknowledgments: We thank all contributors to the Grands Ecosystèmes Lacustres de Tchad (GELT) project, with special thanks to K. Nkouka for hands-on coordination. We thank the national and regional authorities in Chad for welcoming this research. D. Borschneck, D. Delanghe, M. Garcia-Molina, E. Ryken, and Y. Torsy provided laboratory assistance. We further thank the editor and three anonymous reviewers for constructive comments that helped to improve this paper. **Funding:** GELT was funded by the French Ministry of Foreign Affairs as an FSP project (Fonds de Solidarité Prioritaire) and supported by the Ministry of Higher Education, Research and Innovation of Chad, the National Centre for Research and Development in Chad (CNRD), the Chadian universities, and the Service for Cooperation and Cultural Action of the French Embassy. Fieldwork and research was further supported by personal grants to T.V.d.M. from the U.S. National Geographic Society (GEFNE186-16) and the Research Foundation–Flanders. **Author contributions:** T.V.d.M. and D.V. conceptualized the study, interpreted most climate proxy data, and finalized their integration in the manuscript. M.S., P.D., F.S., and M.A. assisted to fieldwork and contributed to data interpretation and manuscript preparation. K.T. and E.B. were in charge of XRF scanning and contributed to its interpretation. T.V.d.M. drafted the paper and prepared figures. E.L.N., L.E.A.O., and Y.A.N. contributed data through MSc thesis research. **Competing interests:** The authors declare that they have no competing interests. **Data and materials availability:** All data needed to evaluate the conclusions in the paper are present in the paper and/or the Supplementary Materials. The Teli Ca/Ti time series is available in the Paleoclimatology Databank of NOAA (https://www.ncei.noaa.gov/access/paleo-search/study/35633).

Submitted 23 July 2021
Accepted 11 February 2022
Published 6 April 2022
10.1126/sciadv.abk1261

ScienceAdvances

A predominantly tropical influence on late Holocene hydroclimate variation in the hyperarid central Sahara

Thijs Van der MeerenDirk VerschurenFlorence SylvestreYacoub A. NassourEvi L. NaudtsLuis E. Aguilar OrtizPierre DeschampsKazuyo TachikawaEdouard BardMathieu SchusterMoussa Abderamane

Sci. Adv., 8 (14), eabk1261. • DOI: 10.1126/sciadv.abk1261